

THE ORIGIN OF THE MASS–METALLICITY RELATION: INSIGHTS FROM 53,000 STAR-FORMING GALAXIES IN THE SDSS

CHRISTY A. TREMONTI^{1,2}, TIMOTHY M. HECKMAN¹, GUINEVERE KAUFFMANN³, JARLE BRINCHMANN^{3,4}, STÉPHANE CHARLOT^{3,5},
SIMON D. M. WHITE³, MARK SEIBERT^{1,6}, ERIC W. PENG^{1,7}, DAVID J. SCHLEGEL⁸, ALAN UOMOTO^{1,9}, MASATAKA FUKUGITA¹⁰, AND
JON BRINKMANN¹¹

Draft version October 22, 2018

ABSTRACT

We utilize Sloan Digital Sky Survey imaging and spectroscopy of $\sim 53,000$ star-forming galaxies at $z \sim 0.1$ to study the relation between stellar mass and gas-phase metallicity. We derive gas-phase oxygen abundances and stellar masses using new techniques which make use of the latest stellar evolutionary synthesis and photoionization models. We find a tight (± 0.1 dex) correlation between stellar mass and metallicity spanning over 3 orders of magnitude in stellar mass and a factor of 10 in metallicity. The relation is relatively steep from $10^{8.5} - 10^{10.5} M_{\odot} h_{70}^{-2}$, in good accord with known trends between luminosity and metallicity, but flattens above $10^{10.5} M_{\odot}$. We use indirect estimates of the gas mass based on the H α luminosity to compare our data to predictions from simple closed box chemical evolution models. We show that metal loss is strongly anti-correlated with baryonic mass, with low mass dwarf galaxies being 5 times more metal-depleted than L* galaxies at $z \sim 0.1$. Evidence for metal depletion is not confined to dwarf galaxies, but is found in galaxies with masses as high as $10^{10} M_{\odot}$. We interpret this as strong evidence both of the ubiquity of galactic winds and of their effectiveness in removing metals from galaxy potential wells.

Subject headings: galaxies: abundances — galaxies: evolution — galaxies: fundamental parameters — galaxies: statistics

1. INTRODUCTION:

Stellar mass and metallicity are two of the most fundamental physical properties of galaxies. Both are metrics of the galaxy evolution process, the former reflecting the amount of gas locked up into stars, and the latter reflecting the gas reprocessed by stars and any exchange of gas between the galaxy and its environment. Understanding how these quantities evolve with time and in relation to one another is central to understanding the physical processes that govern the efficiency and timing of star formation in galaxies.

The influence of stellar winds and supernovae on the interstellar medium (ISM) of galaxies, generally dubbed ‘feedback’, has been regarded as an important ingredient in galaxy evolution since the 1970s (Larson 1974; Larson & Dinerstein 1975; White & Rees 1978). Feedback is believed to play a critical role in regulating star formation by reheating the cold ISM and by physically removing gas from the disk and possibly the halo via galactic winds.

Various lines of observational evidence have established that large-scale outflows of gas are ubiquitous among the most actively star-forming galaxies at low and high redshift (e.g. Lehnert & Heckman 1996; Dahlem, Weaver, & Heckman 1998; Rupke, Veilleux, & Sanders 2002; Shapley et al. 2001; Frye, Broadhurst, & Benítez 2002). However, detailed studies of winds in nearby starbursts have shown them to be a complex, multiphase, hydrodynamical phenomenon with the majority of the energy and newly synthesized metals existing in the hard-to-observe coronal and hot phases ($T = 10^5 - 10^7$ K) (e.g. Strickland et al. 2002). This complexity has prevented both a direct assessment of the cosmological impact of galactic winds, and the development of physically accurate prescriptions for incorporating feedback into semi-analytical and numerical models of galaxy formation.

Fortunately it is possible to obtain some quantitative information about the *impact* of galactic winds without a full understanding of the abstruse physics responsible for their morphology and kinematics. Galaxies which host winds powerful enough to overcome the gravitational binding energy of their halos will vent some of their metals into the intergalactic medium. Hence, one way of evaluating the importance of galactic winds is to look for their chemical imprint on galaxies. However, low metallicity is not necessarily a hallmark of wind activity. The metallicity of a galaxy is expected to depend strongly on its evolutionary state, namely how much of its gas has been turned into stars. To detect metal *depletion* it is therefore necessary to make some assumptions about the expected level of chemical enrichment based on a galaxy’s star and gas content. Of course other mechanisms besides winds could make a galaxy appear to be metal-depleted — for example, the inflow of pristine gas, or the return of comparatively unenriched material from evolved low mass stars. But these scenarios can potentially be distinguished by examining the dependence of metal depletion on dynamical mass. To quantify the impact of feedback on the local galaxy popula-

¹ Department of Physics and Astronomy, The Johns Hopkins University, 3400 N. Charles Street, Baltimore, MD 21218, USA

² Steward Observatory, 933 N. Cherry Ave., Tucson, AZ 85721, USA

³ Max Planck Institut für Astrophysik, Karl-Schwarzschild-Str. 1 Postfach 1317, D-85741 Garching, Germany

⁴ Centro de Astrofísica da Universidade do Porto, Rua das Estrelas - 4150-762 Porto, Portugal

⁵ Institut d’Astrophysique de Paris, CNRS, 98 bis Boulevard Arago, 75914 Paris, France

⁶ Department of Astronomy, California Institute of Technology, 105-24 Caltech, 1201 East California Blvd, Pasadena, CA 91125, USA

⁷ Department of Physics and Astronomy, Rutgers, the State University of New Jersey, 136 Frelinghuysen Road, Piscataway, NJ 08854-8019, USA

⁸ Princeton University Observatory, Peyton Hall, Princeton, NJ 08544-1001, USA

⁹ Carnegie Observatories, 813 Santa Barbara Street Pasadena, California 91101, USA

¹⁰ Institute for Cosmic Ray Research, University of Tokyo, Kashiwa 277-8582, Japan

¹¹ Apache Point Observatory, PO Box 59, Sunspot, NM 88349, USA

tion we therefore compare the observed metallicities of galaxies spanning a wide range in total mass to the predictions of simple chemical evolution models.

Interest in the relationship between mass and metallicity dates back several decades, beginning with the seminal work of Lequeux et al. (1979). However, because of the difficulty of obtaining masses, luminosity was generally adopted as a surrogate. A correlation between metallicity and blue luminosity was demonstrated by Garnett & Shields (1987) and extended by various authors (e.g Skillman, Kennicutt, & Hodge 1989; Brodie & Huchra 1991; Zaritsky, Kennicutt, & Huchra 1994) to include a range of Hubble types and to span over 11 magnitudes in luminosity and 2 dex in metallicity. The interpretation of this striking trend has, however, remained a matter of some debate owing to the difficulty of transforming from observables to the ingredients needed for simple chemical evolution models (stellar mass, gas mass, and metallicity).

In recent years, the development of more sophisticated models for stellar populations (e.g. Bruzual & Charlot 2003) and gaseous nebulae (e.g. Ferland 1996; Charlot & Longhetti 2001) has resulted in major advances in our ability to derive physical properties from observables. In this work we derive stellar mass-to-light (M/L) ratios according to the methods of Kauffmann et al. (2003a) which rely on spectroscopic line indices to help circumvent the classical age-metallicity-reddening degeneracy issues. We measure metallicity using the formalism of Charlot et al. (2004) which makes use of all of the strong optical nebular lines in our bandpass (as opposed to more traditional methods which rely on a single line ratio.) We couple these improved techniques with the enormous statistical power provided by the Sloan Digital Sky Survey (SDSS). We present the mass-metallicity relation of $\sim 53,000$ star-forming galaxies at $z \sim 0.1$ as a new benchmark for successful models of galaxy evolution.

We begin with a brief description of the SDSS data products and our data processing techniques in §2. We outline our method for measuring metallicity and stellar mass in §3. In §4 we compare the luminosity-metallicity relation of the SDSS data with previous determinations. We present the mass-metallicity relationship in §5 and consider its origin in §6. We explore sources of systematic error in §7 and conclude in §8. Where appropriate we adopt a cosmology of $\Omega_M = 0.3$, $\Omega_\Lambda = 0.7$, and $H_0 = 70 \text{ km s}^{-1} \text{ Mpc}^{-1}$.

2. THE SDSS DATA

The data analyzed in this study are drawn from the Sloan Digital Sky Survey (SDSS). The survey goals are to obtain photometry of a quarter of the sky and spectra of nearly one million objects. Imaging is obtained in the u , g , r , i , z bands (Fukugita et al. 1996; Smith et al. 2002) with a special purpose drift scan camera (Gunn et al. 1998) mounted on the SDSS 2.5 meter telescope at Apache Point Observatory. The imaging data are photometrically (Hogg et al. 2001) and astrometrically (Pier et al. 2003) calibrated, and used to select stars, galaxies, and quasars for follow-up fiber spectroscopy. Spectroscopic fibers are assigned to objects on the sky using an efficient tiling algorithm designed to optimize completeness (Blanton et al. 2003a). The details of the survey strategy can be found in York et al. (2000) and an overview of the data pipelines and products is provided in the Early Data Release paper (Stoughton et al. 2002).

Our parent sample for this study is composed of 211,265 objects which have been spectroscopically confirmed as galaxies and have data publicly available in the SDSS Data

Release 2 (DR2; Abazajian et al. 2004). These galaxies are part of the SDSS ‘main’ galaxy sample used for large scale structure studies (Strauss et al. 2002) and have Petrosian r magnitudes in the range $14.5 < r < 17.77$ after correction for foreground galactic extinction using the reddening maps of Schlegel, Finkbeiner, & Davis (1998). Their redshift distribution extends from ~ 0.005 to 0.30, with a median z of 0.10. From this sample we select a subset of 53,400 star-forming galaxies for nebular analysis, as discussed in §2.2.

We determine stellar mass-to-light ratios and nebular metallicities for our sample galaxies from the SDSS spectra. The spectra are obtained with two 320-fiber spectrographs mounted on the SDSS 2.5-meter telescope. Fibers $3''$ in diameter are manually plugged into custom-drilled aluminum plates mounted at the focal plane of the telescope. The spectra are exposed for 45 minutes or until a fiducial signal-to-noise (S/N) is reached. The median S/N per pixel for galaxies in the main sample is ~ 14 . The spectra are processed by an automated pipeline (Schlegel et al., in prep.) which flux and wavelength calibrates the data from 3800 to 9200 Å. The instrumental resolution is $R \equiv \lambda/\delta\lambda = 1850 - 2200$ (FWHM ~ 2.4 Å at 5000 Å).

The wavelength coverage, resolution, S/N, and general high quality of the SDSS spectra make them extremely well suited for the derivation of nebular abundances. However the spectrophotometric calibration and the small size of the fiber aperture relative to the target galaxies pose some concern. The SDSS spectrographs do not employ an atmospheric dispersion corrector and the spectra are frequently acquired under non-photometric conditions. The Survey has nevertheless been able to obtain a remarkable level of spectrophotometric precision by the simple practice of observing multiple standard stars simultaneously with the science targets. (The artifice in this case is that the ‘standards’ are not classical spectrophotometric standards, but are halo F-subdwarfs that are calibrated to stellar models – see Abazajian et al. (2004) for details.) To quantify the quality of the spectrophotometry we have compared magnitudes synthesized from the spectra with SDSS photometry obtained with an aperture matched to the fiber size. The 1σ error in the synthetic colors is 5% in $g-r$ and 3% in $r-i$ ($\lambda_g \sim 4700$ Å; $\lambda_r \sim 6200$ Å; $\lambda_i \sim 7500$ Å). At the bluest wavelengths (~ 3800 Å) we estimate the error to be $\sim 12\%$ based on repeat observations. There is also a systematic error in the sense that the spectra are bluer than the imaging by $\sim 2\%$ in the g -band, but it is unclear at present whether this represents an error in the absolute calibration of the photometry or the spectroscopy. While the random errors in the spectrophotometry are offset by the large size of the data set, the accuracy of our measured nebular abundances relative to true global abundances is compromised to some degree by the size of the fiber aperture. At the median redshift of the SDSS main galaxy sample ($z \sim 0.1$) the target galaxies subtend several arcseconds on the sky. The fraction of galaxy light falling in the $3''$ fiber aperture is typically about 1/3, with variations in redshift and morphological type causing the fraction to range from 0.05 – 0.6. The impact of this ‘aperture bias’ is discussed in §7.

2.1. Emission Line Measurement

The emphasis of this study is on the nebular emission line spectra of galaxies. However, we can not disregard the fact that the optical spectra of galaxies are very rich in stellar *absorption* features, which can complicate the measurement of

nebular emission lines. In order to maintain speed and flexibility, the SDSS spectroscopic pipeline performs a very simple estimate of the stellar continuum using a sliding median. While this is generally adequate for strong emission lines, a more sophisticated treatment of the continuum is required to recover weak features and to properly account for the stellar Balmer absorption which can reach equivalent widths of 5 \AA in some galaxies. To address this need, we have designed a special-purpose code optimized for use with SDSS galaxy spectra which fits a stellar population model to the continuum. We adopt the basic assumption that any galaxy star formation history can be approximated as a sum of discrete bursts. Our library of template spectra is composed of single stellar population models generated using the new population synthesis code of Bruzual & Charlot (2003, hereafter BC03). The BC03 models incorporate an empirical spectral library (Le Borgne et al. 2003) with a wavelength coverage ($3200 - 9300 \text{ \AA}$) and spectral resolution ($\sim 3 \text{ \AA}$) which is well matched to that of the SDSS data. Our templates include models of ten different ages (0.005, 0.025, 0.1, 0.2, 0.6, 0.9, 1.4, 2.5, 5, 10 Gyr) and three metallicities ($1/5 Z_{\odot}$, Z_{\odot} , and $2.5 Z_{\odot}$). For each galaxy we transform the templates to the appropriate redshift and velocity dispersion and resample them to match the data. To construct the best fitting model we perform a non-negative least squares fit with dust attenuation modeled as an additional free parameter. In practice, our ability to simultaneously recover ages and metallicities is strongly limited by the signal-to-noise of the data. Hence we model galaxies as single metallicity populations and select the metallicity which yields the minimum χ^2 . (While this is not particularly physical, in practice it is not a bad assumption since the integrated light of a galaxy tends to be dominated by the light of its most recent stellar generation.) The details of the template fitting code will be presented in Tremonti et al. (in prep.). Figure 1 shows some typical spectra and their continuum models.

After subtracting the best-fitting stellar population model of the continuum, we remove any remaining residuals (usually of order a few percent) with a sliding 200 pixel median, and fit the nebular emission lines. Since we are interested in recovering very weak nebular features, we adopt a special strategy: we fit all the emission lines with Gaussians simultaneously, requiring that all of the Balmer lines ($H\delta$, $H\gamma$, $H\beta$, and $H\alpha$) have the same line width and velocity offset, and likewise for the forbidden lines ($[\text{O II}] \lambda\lambda 3726, 3729$, $[\text{O III}] \lambda\lambda 4959, 5007$, $[\text{N II}] \lambda\lambda 6548, 6584$, $[\text{S II}] \lambda\lambda 6717, 6731$). We are careful to take into account the wavelength-dependent instrumental resolution of each fiber, which is measured for each set of observations by the SDSS spectroscopic pipeline from the arc lamp images. The virtue of constraining the line widths and velocity offsets is that it minimizes the number of free parameters and effectively allows the stronger lines to be used to help constrain the weaker ones. Extensive by-eye inspection suggests that our continuum and line fitting methods work well.

2.2. The Galaxy Sample

From our original sample of $\sim 211,000$ galaxies, we select a subsample of star-forming galaxies for nebular analysis. We start by imposing a redshift cut of $0.005 < z < 0.25$, and requiring that $> 10\%$ of the total galaxy light be observed by the fiber. Because stellar mass and metallicity are derived using Bayesian techniques (see §3), it would be possible to select a

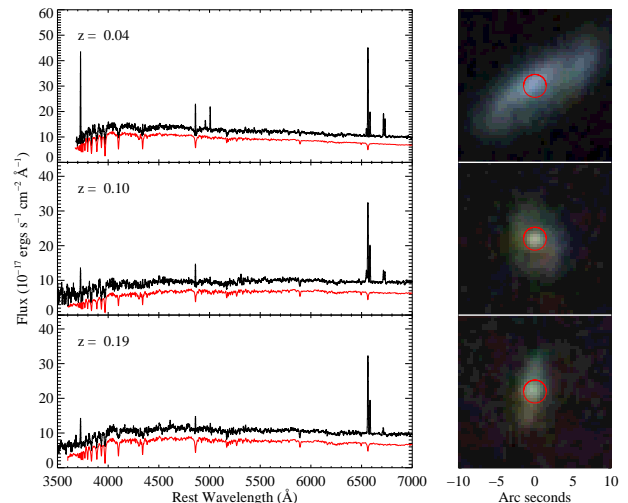


FIG. 1.— Images and spectra of some typical galaxies in our sample at a range of redshifts. The red circle on the images denotes the fiber aperture. The continuum model for each spectrum is shown in red and offset slightly for clarity. The continuum model is constructed from the Bruzual & Charlot (2003) stellar population synthesis models as described in §2.1. Both observed and model spectra have been smoothed by 5 pixels.

sample of objects with accurate masses and metallicities using the likelihood distributions. However, for clarity we have opted to define our sample based on observables (line fluxes, line indices) and later make some weak cuts based on the derived parameters. We require galaxies included in our star-forming sample to have lines of $H\beta$, $H\alpha$, and $[\text{N II}] \lambda 6584$ detected at greater than 5σ . We do not explicitly constrain the other nebular lines that we make use of ($[\text{O II}] \lambda\lambda 3726, 3729$, $[\text{O III}] \lambda 5007$, $\text{He I } \lambda 5876$, $[\text{O I}] \lambda 6300$, $[\text{S II}] \lambda\lambda 6717, 6731$) because our Bayesian analysis takes into account the errors in the line fluxes. We note that $[\text{O II}]$ is not measured at $z < 0.03$ due to the blue wavelength cut-off of the spectrographs. This affects 5% of our sample but has a negligible impact on our nebular analysis due to the use of multiple lines (see §3.1). We impose the requirement that the parameters needed for mass determination have small errors (see §3.2). These criteria are: $\sigma(m_z) < 0.15 \text{ mag}$, $\sigma(H\delta_A) < 2.5 \text{ \AA}$, and $\sigma[D_n(4000)] < 0.1$. The combination of these constraints trims the sample to $\sim 82,000$ galaxies, with the limiting factor typically being the strength of the $H\beta$ line.

We remove galaxies harboring an Active Galactic Nucleus (AGN) from our sample using the traditional line diagnostic diagram $[\text{N II}]/H\alpha$ versus $[\text{O III}]/H\beta$ (Baldwin, Phillips, & Terlevich 1981; Veilleux & Osterbrock 1987). The division between star-forming galaxies and AGN has been calibrated theoretically by Kewley et al. (2001). We adopt the slightly modified formula used by Kauffmann et al. (2003c) which provides a more conservative approach to selecting star-forming galaxies (see their Fig. 1). We apply this criterion where we detect $[\text{O III}]$ with 3σ sigma significance (and $H\beta$, $H\alpha$, and $[\text{N II}]$ at 5σ , as specified earlier.) To avoid biasing ourselves against high metallicity galaxies which have intrinsically weak $[\text{O III}]$, we also include objects with $[\text{O III}] < 3\sigma$ and $\log([\text{N II}]/H\alpha) < -0.4$ in our star-forming sample. These galaxies comprise $\sim 16\%$ of our final sample. The fraction of emission line galaxies that we reject because of AGN contamination is $\sim 33\%$.

Finally, we require the 1σ errors in stellar mass and metallicity derived from the likelihood distributions to be less than 0.2 dex. This cut eliminates 3% of the remaining galaxies, leaving us with a sample of 53,400 galaxies. Some example galaxies and their spectra are shown in Figure 1. The redshift, luminosity, color, and morphology of our star-forming sample is compared with that of the DR2 main galaxy sample in Figure 2. We use the concentration index, C , as a rough proxy for galaxy morphology. It is defined as the ratio of the radii enclosing 90% and 50% of the Petrosian r -band galaxy light ($C = R_{90}/R_{50}$). Shimasaku et al. (2001) and Strateva et al. (2001) have shown that there is a good correspondence between C and Hubble type, with $C \sim 2.6$ marking the boundary between early- and late-types. As expected, our emission line sample has bluer colors and more late-type morphologies than the parent sample. The redshift distribution is similar to that of the main survey, and peaks around $z = 0.08$.

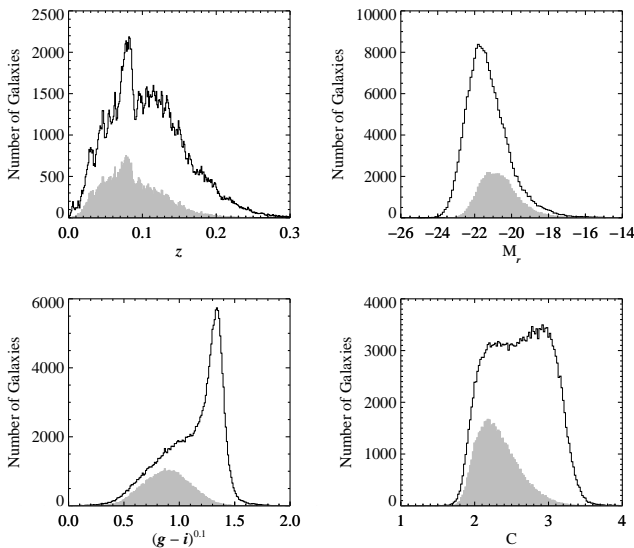


FIG. 2.— Properties of the SDSS main sample and our star-forming galaxy sample (gray shaded histograms). The upper left panel shows the redshift distribution. The upper right panel shows absolute r -band Petrosian magnitudes. The lower left panel shows the distribution of galaxy $(g-i)$ color. The colors have been k -corrected to $z = 0.1$ following Blanton et al. (2003b). The lower right panel shows the concentration index, $C = R_{90}/R_{50}$. Concentration correlates loosely with Hubble type, with $C \sim 2.6$ marking the boundary between early- and late-types.

3. THE PHYSICAL PROPERTIES OF GALAXIES

3.1. Measuring Metallicity

We derive oxygen abundances for our SDSS galaxies from the optical nebular emission lines. There are a number of advantages of measuring metallicity¹² from the nebular lines rather than the stellar absorption features via Lick indices (Worthey 1994). First, the S/N in the emission lines can greatly exceed that in the continuum, with the added advantage that many of the optically faintest galaxies (dwarfs) exhibit the highest emission line equivalent widths. Secondly, nebular abundance determination is free of the uncertainties due to age and α -element enhancement which plague the interpretation of absorption line indices. Thirdly, nebular metallicities are easier to interpret in the context of chemical evolution models because they reflect the present-day metal abundance rather than the luminosity-weighted average of previ-

ous stellar generations. The disadvantage is that our analysis is limited to galaxies with on-going star formation.

The strong optical nebular lines of elements other than H and He are produced by collisionally excited transitions. The strength of these lines is the product not only of the heavy element abundance, but the temperature, density, and ionization state of the nebula, the attenuation by dust, and the depletion of metals on to dust grains. In practice, direct determination of element abundances from optical emission lines tends to be limited by the faintness of the [O III] $\lambda 4363$ line which is used to determine the electron temperature. When the electron temperature cannot be measured directly, oxygen abundances can be estimated using empirically or theoretically calibrated relations between metallicity and the relative fluxes of various strong optical emission lines. ‘Strong-line’ abundance calibration was pioneered by Alloin et al. (1979) and Pagel et al. (1979). The latter introduced the R_{23} metallicity indicator ($R_{23} = ([\text{O II}] \lambda 3727 + [\text{O III}] \lambda \lambda 4959, 5007) / \text{H}\beta$) which has enjoyed widespread use. Various other line ratios have been calibrated as metallicity indicators, including [N II] $\lambda 6584 / \text{H}\alpha$, [O III] $\lambda 5007 / [\text{N II}] \lambda 6584$, [N II] $\lambda 6584 / [\text{O II}] \lambda 3727$, and $([\text{S II}] \lambda \lambda 6717, 6731 + [\text{S III}] \lambda \lambda 90069, 9532) / \text{H}\beta$. Systematic differences among the various strong-line calibrations can exceed 0.2 dex. (See Kewley & Dopita 2002 for a review).

Here we measure metallicities in a slightly more refined way, using the approach outlined by Charlot et al. (2004). This consists of estimating metallicity statistically, based on simultaneous fits of all the most prominent emission lines ([O II], H β , [O III], He I, [O I], H α , [N II], [S II]) with a model designed for the interpretation of integrated galaxy spectra (Charlot & Longhetti 2001). The Charlot & Longhetti (2001) model is based on a combination of the Bruzual & Charlot (1993) and Ferland (1996, version C90.04) population synthesis and photoionization codes. In this model, the contributions to the nebular emission by H II regions and diffuse ionized gas are combined and described in terms of an effective (i.e. galaxy-averaged) metallicity, ionization parameter, dust attenuation at 5500 Å, and dust-to-metal ratio. The depletion of heavy elements onto dust grains and the absorption of ionizing photons by dust are included in a self-consistent way. Charlot & Longhetti (2001) calibrated the emission-line properties of their model using the observed [O III]/H β , [O II]/[O III], [S II]/H α and [N II]/[S II] ratios of a representative sample of 92 nearby spiral, irregular, starburst, and H II galaxies. The model also accounts well for the properties of these lines in our sample (Brinchmann et al. 2004, Fig. 5). We calculate the likelihood distribution of the metallicity of each galaxy in our sample, based on comparisons with a large library of models ($\sim 2 \times 10^5$) corresponding to different assumptions about the effective gas parameters. We adopt the median of this distribution as our best estimate of the galaxy metallicity; the width of the likelihood distribution provides a measure of the error. The median 1σ error for our sample of star-forming galaxies is 0.03 dex. We note that this

¹² The word ‘metallicity’ has been used variously in the literature. In stellar studies metallicity usually refers to the iron abundance. Oxygen has been adopted as the canonical ‘metal’ for ISM studies because it is the most abundant, it is only weakly depleted on to dust grains, and it displays strong lines in the optical. Hereafter we use metallicity to denote the gas-phase oxygen abundance measured in units of $12 + \log(\text{O}/\text{H})$, where the ratio O/H is the abundance by number of oxygen relative to hydrogen. Solar metallicity in these units is 8.69 (Allende Prieto, Lambert, & Apslund 2001) and LMC and SMC metallicity are 8.4 and 8.0, respectively (Garnett 1999).

does not include systematic error. Because our metallicities are discretely sampled, we have added small random offsets for display purposes. These have a Gaussian distribution with $\sigma = 0.02$ dex.

Our models implicitly assume that the nebular gas in a galaxy can be characterized by a set of galaxy-averaged physical properties. An important issue is whether truly representative abundances can be derived for spatially integrated galaxy spectra in the presence of radial variations in temperature, ionization, metallicity, and dust extinction (Vila-Costas & Edmunds 1992; Zaritsky, Kennicutt, & Huchra 1994; Martin & Roy 1994; van Zee et al. 1998). Kobulnicky, Kennicutt, & Pizagno (1999) addressed this issue by comparing H II region abundances at particular disk radii with abundances measured from integrated spectra. They found excellent agreement (± 0.05 dex) when metallicities were based on R_{23} . However, the study is limited in one respect: they use weighted averages of the H II region spectra as proxies for true integrated spectra, thereby ignoring the contribution of the diffuse ionized gas which can be responsible for 25 - 70% of the Balmer line emission (Martin 1997; Zurita, Rozas, & Beckman 2000; Thilker, Walterbos, Braun, & Hoopes 2002). Hence further study is needed to quantify the systematics associated with true integrated abundances.

To place our metallicity measurements in the context of previous work, we show the relation between our derived metallicities and the line ratio $R_{23} = ([\text{O II}] + [\text{O III}]) / \text{H}\beta$ in Figure 3. For comparison we show the theoretical relation between R_{23} and metallicity derived by McGaugh (1991)¹³, the empirical relation defined by Edmunds & Pagel (1984), and the semi-empirical relation of Zaritsky, Kennicutt, & Huchra (1994), itself an average of 3 previous calibrations (Dopita & Evans 1986; Edmunds & Pagel 1984; McCall, Rybski, & Shields 1985). These analytic R_{23} -metallicity relations roughly bracket the range of metallicities that we derive, showing that our measurements are in line with previous strong-line calibrations. However, recent work suggests that strong-line methods may overestimate oxygen abundances *systematically* by as much as a factor of two (Kennicutt, Bresolin, & Garnett 2003).

The strength of our Bayesian metallicity estimates is that they make use of all of the available nebular lines rather than relying on a small subset of them, as is the case for R_{23} . However, full spectral modeling is not always possible or practical. Hence we provide an analytical fit to the R_{23} -metallicity relation shown in Figure 3:

$$12 + \log(\text{O}/\text{H}) = 9.185 - 0.313x - 0.264x^2 - 0.321x^3, \quad (1)$$

where $x \equiv \log R_{23}$. This formula is valid for the upper branch of the double-valued R_{23} -abundance relation. The lower branch is not very well sampled by our data. We measure metallicities below $12 + \log(\text{O}/\text{H}) = 8.5$ for 940 galaxies. However less than 1/3 of these can be plotted in Figure 3 because most are at such low redshift that $[\text{O II}] \lambda 3727$ is not in our spectroscopic bandpass. While galaxies lacking $[\text{O II}]$ have larger errors associated with their derived abundances, they show trends between abundance and luminosity that are generally consistent with the rest of the sample.

3.2. Measuring Stellar Mass

¹³ We use the analytic formula for the relation between R_{23} and metallicity reported in Kobulnicky, Kennicutt, & Pizagno (1999).

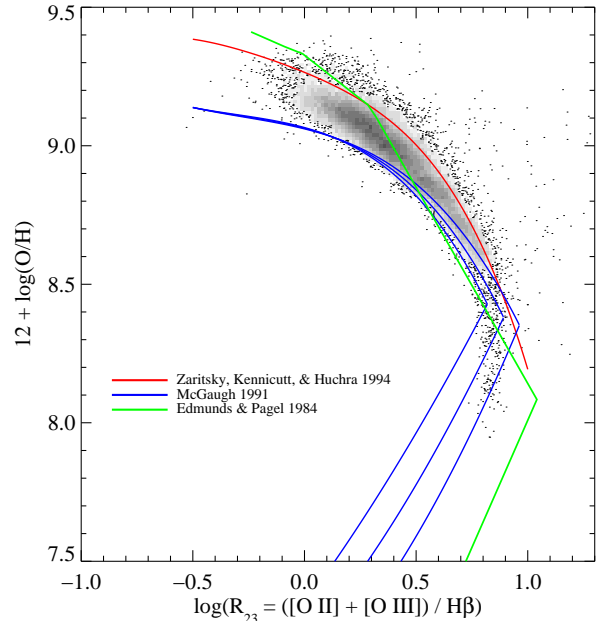


FIG. 3.— Comparison of the relation between metallicity and the line ratio $R_{23} = ([\text{O II}] + [\text{O III}]) / \text{H}\beta$. In this and subsequent figures we represent the SDSS data using a combination of a two dimensional histogram and plotted points. We histogram the data where more than 5 data points fall in an individual pixel, and plot it as individual points otherwise. The histograms have been square-root scaled for better visibility. Metallicities for the SDSS data have been derived using statistical methods described in the text. The blue line shows the theoretical calibration of McGaugh (1991) (as reported in Kobulnicky, Kennicutt, & Pizagno (1999)) for three representative values of $[\text{O III}]/[\text{O II}]$. The green line shows the empirical calibration of Edmunds & Pagel (1984), and the red line shows the semi-empirical calibration of Zaritsky, Kennicutt, & Huchra (1994), itself the average of 3 previous calibrations.

The stellar mass of a galaxy cannot be inferred directly from its optical luminosity because the stellar mass-to-light ratio depends strongly on the galaxy's star formation history and metallicity. Optical colors have been widely used to estimate M/L ratios (e.g. Bell & de Jong 2001; Brinchmann & Ellis 2000). However, errors in the derived M/L are known to result if galaxies have formed a substantial fraction ($> 10\%$) of their stars in a recent burst. This caveat is particularly problematic given our sample of actively star-forming galaxies. We therefore adopt the method of Kauffmann et al. (2003a) for deriving stellar masses. This method relies on spectral indicators of the stellar age and the fraction of stars formed in recent bursts. As our present sample is actually an extension of Kauffmann's, we provide only a cursory description of our methods here.

We use the z -band ($\lambda \sim 8900 \text{ \AA}$) magnitude to characterize the galaxy luminosity because it is less sensitive than the bluer bands to extinction and the age of the stellar population. However, even in this near-infrared passband the M/L ratio is not a constant, but can vary by up to a factor of 10 when a full range of star formation histories is considered (Kauffmann et al. 2003a, see Fig. 4). Constraints on the star formation history are provided by the spectral indices $D_n(4000)$ and $\text{H}\delta_A$, which measure the 4000 \AA break and the stellar Balmer absorption. The location of a galaxy in the $D_n(4000)$ - $\text{H}\delta_A$ plane is insensitive to reddening, and only weakly dependent on metallicity; however, it is a powerful diagnostic of whether the galaxy has

been forming stars continuously or in bursts over the past 1 - 2 Gyr. We assign stellar M/L ratios to our galaxies by using a Bayesian analysis to associate the observed $D_n(4000)$ and $H\delta_A$ values with a model drawn from a large library of Monte Carlo realizations of galaxies with different star formation histories and metallicities. A comparison with broadband photometry then yields estimates of the dust attenuation and the stellar mass. Errors in our masses are estimated from the width of the likelihood distribution. The median 1σ error for our sample of star-forming galaxies is 0.09 dex. Our masses assume a Kroupa (2001) Initial Mass Function (IMF).

4. THE LUMINOSITY–METALLICITY RELATIONSHIP

Because of the relative difficulty of measuring the stellar mass of galaxies, most previous work has focused on the relationship between galaxy luminosity and metallicity. Following the pioneering work of Lequeux et al. (1979), Skillman, Kennicutt, & Hodge (1989) established a luminosity–metallicity relation for irregular galaxies which was confirmed by Richer & McCall (1995) and extended to spiral galaxies by Garnett & Shields (1987), Vila-Costas & Edmunds (1992), Zaritsky, Kennicutt, & Huchra (1994), and Kobulnicky & Zaritsky (1999). Recently attempts have been made to provide better comparison samples for high redshift by studying the luminosity–metallicity relation in starburst nuclei (Coziol, Contini, Davoust, & Considere 1997), and UV-selected (Contini et al. 2002) and emission line-selected samples (Melbourne & Salzer 2002).

It is instructive to compare the luminosity–metallicity relation of our sample with previous work, both to validate the consistency of our measurements and to elucidate the effects of our sample selection. Although redder bandpasses are less sensitive to the effects of dust obscuration and recent starbursts, historical precedent mandates that the luminosity–metallicity relationship be presented in terms of absolute B magnitude. Fortunately, the SDSS g band is fairly similar to the Johnson B band. We adopt the transformation given in Smith et al. (2002) and k -correct the magnitudes to $z = 0$ using the `kcorrect` code of Blanton et al. (2003b). We correct our measured blue luminosities for galactic foreground extinction (Schlegel, Finkbeiner, & Davis 1998) and for inclination dependent intrinsic attenuation (Tully et al. 1998). The latter implies a correction to a face-on orientation, but does *not* account for the intrinsic attenuation in a face-on system. The median correction is $A_B^{inc} = 0.3$ mag.

Figure 4 shows the luminosity–metallicity relation of the SDSS galaxies and various samples from the literature. We have corrected the published B-band luminosities to our adopted value of H_0 where appropriate, but we have made no attempt to homogenize the metallicities to account for the different calibrations used. In comparing SDSS data with other samples, it is important to consider the possible aperture bias. We expect our metallicity measurements to slightly overestimate the true global abundances, as discussed further in §7. However, in view of the different metallicity calibrations used, the magnitude of this offset is probably not the dominant systematic effect. The SDSS data show generally good agreement with other local samples of galaxies, albeit with a paucity of dwarfs.

In keeping with previous work, we fit the luminosity–metallicity relation using a linear least squares technique. The measurement errors in luminosity (± 0.01 dex) and metallicity (± 0.1 dex) are small compared to the observed scatter. The

traditional method of estimating the underlying functional relation in this case is to use the linear bisector — the line which bisects the ordinary least-squares regression of X vs. Y and Y vs. X (Isobe, Feigelson, Akritas, & Babu 1990). The luminosity–metallicity relation for our galaxies fitted in this manner is

$$12 + \log(\text{O}/\text{H}) = -0.185(\pm 0.001)M_B + 5.238(\pm 0.018). \quad (2)$$

Our measured slope is intermediate between that found by Kobulnicky & Zaritsky (1999) for local irregulars and spirals and that measured by Melbourne & Salzer (2002) for a subset of galaxies from the KPNO International Spectroscopic Survey (KISS). In inter-comparing data sets it is important to note that different authors (including the two mentioned above) have adopted different regression methods. Different regression methods calculate intrinsically different properties of the data and *are not directly comparable* (see Isobe, Feigelson, Akritas, & Babu (1990) for a full discussion). Figure 4 therefore elucidates the differences in the measured luminosity–metallicity relation which are the result of sample selection, metallicity calibration, and data characterization (fitting). All of these factors need to be carefully considered when looking for evidence of evolution in the luminosity–metallicity relation.

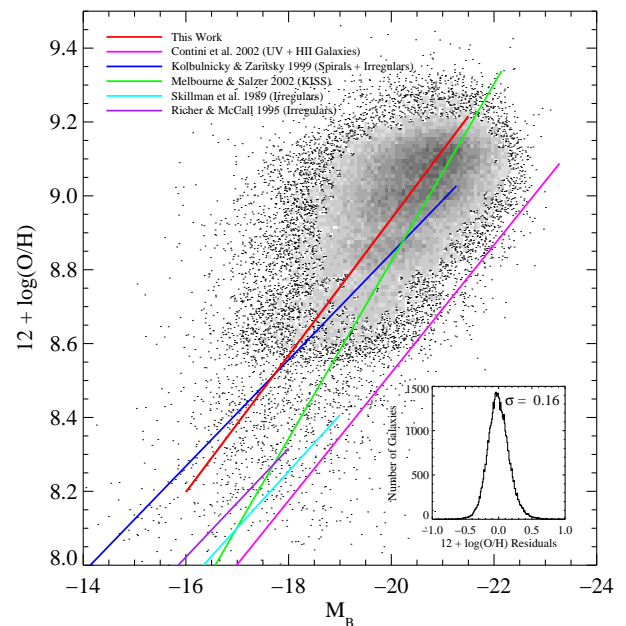


FIG. 4.— The luminosity–metallicity relation for SDSS galaxies and various galaxy samples drawn from the literature (see legend). All of the B magnitudes have been corrected to $H_0 = 70 \text{ km s}^{-1} \text{ Mpc}^{-1}$, but we have made no attempt to homogenize the metallicity measurements. The red line represents the linear least squares bisector fit to the SDSS data. The inset plot shows the residuals of the fit.

At fixed metallicity, the SDSS galaxies span more than 4 magnitudes in blue luminosity. The brightest galaxies are consistent with the luminosity–metallicity relation found by Contini et al. (2002) for a sample of UV-selected galaxies (pink line in Fig. 4). Contini et al. postulate that these galaxies are offset from the luminosity–metallicity relation of normal spirals due to the low M/L ratio of their newly formed stellar populations. This suggests a physical origin for the scatter, an idea that we explore further in Figure 5. To reduce sources of

measurement error, we switch to using the luminosity in the native SDSS passbands, k -corrected to the median redshift, $z \sim 0.1$. To quantify the influence of dust, we correct the galaxy luminosities for intrinsic attenuation using the attenuation curve of Charlot & Fall (2000) and assuming that the stars experience 1/3 of the attenuation measured in the nebular gas. The nebular attenuation is determined simultaneously with the metallicity assuming a metallicity-dependent Case B $H\alpha/H\beta$ ratio (Brinchmann et al. 2004; Charlot et al. 2004). We assume that the correction for intrinsic attenuation automatically accounts for any inclination-dependent effects.

In Figure 5 we systematically examine the impact of dust and M/L variations on the luminosity–metallicity relation by adopting different measures of galaxy luminosity: 1) the absolute g -band magnitude corrected for inclination-dependent attenuation following Tully et al. (1998); 2) the absolute g -band magnitude corrected for intrinsic attenuation, as described above; 3) and the absolute z -band magnitude corrected for intrinsic attenuation. In panels 1-3 of Figure 5 we indicate the *distribution* of metallicity at a given luminosity by displaying the contours which enclose 68 and 95% of the data in bins of 0.4 mag. The contours provide a non-parametric description of the distribution which is unbiased as long as the errors in luminosity are small relative to our adopted bin-size. For comparison, we also show the traditional least-squares linear bisector fit to the data in panel 1 ($12+\log(\text{O}/\text{H}) = -0.186(\pm 0.001)M_g + 5.195(\pm 0.018)$). Because we do not know a priori the true functional form of the luminosity–metallicity relation, we focus on the contours. Comparison of the first two panels of Figure 5 shows that correcting the luminosity for attenuation reduces the scatter and flattens the luminosity–metallicity relation at high mass. This trend is even more pronounced when the extinction corrected z -band magnitude is used (panel 3). Because the z -band is less sensitive to dust and recent starbursts, the range of M/L ratios is smaller, and the scatter is reduced by $\sim 20\%$ compared to the uncorrected g -band. However, even in the z -band, M/L ratios can vary by factors of a few. This effect is illustrated in panel 4 where we plot the median z -band luminosity–metallicity relation for galaxies in four bins of $D_n(4000)$. As discussed in Kauffmann et al. (2003a), $D_n(4000)$ is a good measure of the mean stellar age of the population. Our interpretation of panel 4 is that at fixed metallicity, galaxies with lower $D_n(4000)$ are shifted to brighter magnitudes because of the lower M/L ratios of their young stellar populations. This confirms our intuition that the underlying physical correlation is between stellar mass and metallicity.

5. THE MASS–METALLICITY RELATIONSHIP

With our new prescriptions for measuring stellar mass and gas-phase metallicity it is now possible to examine the mass–metallicity relationship of our sample of SDSS star-forming galaxies. Figure 6 shows that a striking correlation is observed, extending over 3 decades in stellar mass and a factor of 10 in metallicity. The correlation is roughly linear from $10^{8.5} M_\odot$ to $10^{10.5} M_\odot$ after which a gradual flattening occurs. Most remarkable of all is the tightness of the correlation: the 1σ spread of the data about the median is ± 0.10 dex, with only a handful of extreme outliers present. The relationship is well fitted by a polynomial of the form:

$$12+\log(\text{O}/\text{H}) = -1.492 + 1.847(\log M_*) - 0.08026(\log M_*)^2 \quad (3)$$

where M_* represents the stellar mass in units of solar masses. This equation is valid over the range $8.5 < \log M_* < 11.5$.

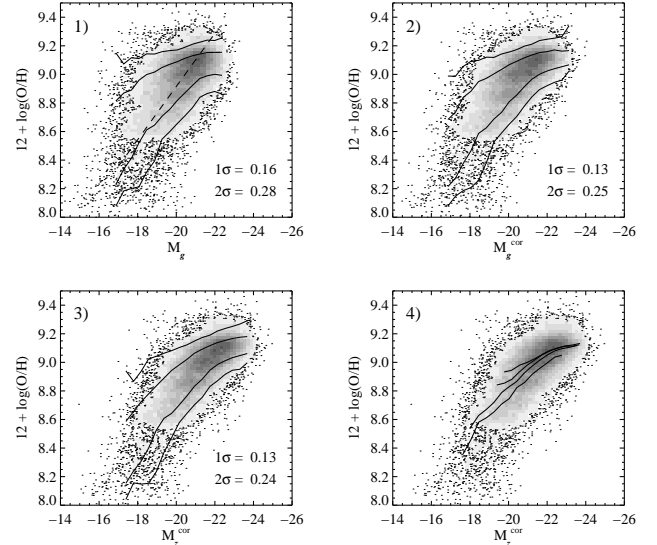


FIG. 5.— The luminosity–metallicity relation of SDSS galaxies in the g and z -bands. In the first panel we have corrected M_g to face-on orientation, but we have not corrected for internal attenuation. In panels 2-4 we correct M_g and M_z for internal attenuation, assuming that the stars experience 1/3 of the reddening measured in the gas. The solid black contours in panels 1-3 enclose 68 and 95% of data with statistics computed in bins of 0.4 mag in luminosity. The median half-width of the distribution is listed in the lower right corner. For comparison, the dashed line in the first panel shows the least-squares linear bisector fit to the data. The fourth panel shows the median z -band luminosity–metallicity relation for galaxies in four bins of $D_n(4000)$: from bottom to top, 1.0 - 1.2, 1.2 - 1.3, 1.3 - 1.4, 1.4 - 1.8. Data for the contours in panels 1 and 3 are given in Tables 1 and 2.

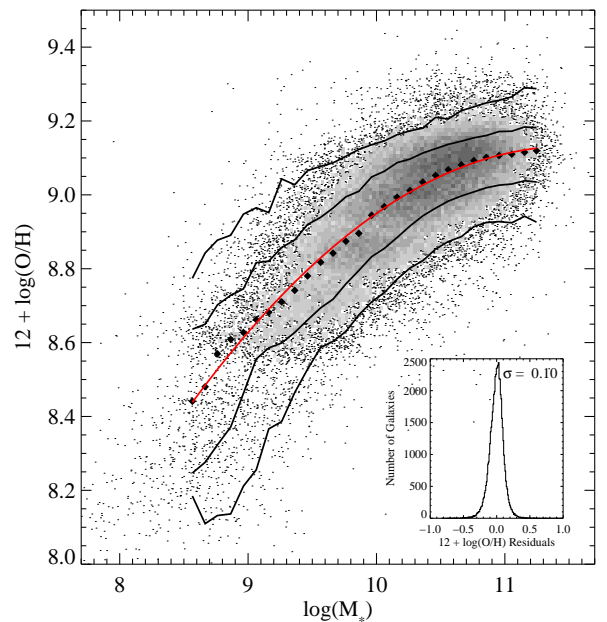


FIG. 6.— The relation between stellar mass, in units of solar masses, and gas-phase oxygen abundance for $\sim 53,400$ star-forming galaxies in the SDSS. The large black points represent the median in bins of 0.1 dex in mass which include at least 100 data points. The solid lines are the contours which enclose 68% and 95% of the data. The red line shows a polynomial fit to the data. The inset plot shows the residuals of the fit. Data for the contours are given in Table 3.

The principal difference between the mass–metallicity

and luminosity–metallicity relations is the more pronounced turnover seen at high metallicity when mass is used as the independent variable. In Figure 5 we demonstrated that both dust and M/L variations act to smear out the turnover when luminosity is used in place of mass. Accordingly, the scatter in the uncorrected g -band luminosity–metallicity relation is $\sim 50\%$ higher than the scatter in the mass–metallicity relation.

We emphasize that the turnover in the mass–metallicity relation is not an artifact of our metallicity calibration. As shown in Figure 3 our metallicity estimates are consistent with other strong-line calibrations. If we adopt the R_{23} metallicity calibration of Zaritsky, Kennicutt, & Huchra (1994), the shape of the mass–metallicity relation is well reproduced, but the scatter increases by $\sim 15\%$. Use of the McGaugh (1991) R_{23} metallicity calibration results in a *more* pronounced turnover, due to the flatter relation between R_{23} and $\log(O/H)$.

The shape of the mass–metallicity relation is also robust with respect to our choice of S/N cuts. The S/N in the $H\beta$ line is generally the parameter that drives our galaxy selection. The main concern is that our requirement of $(S/N)_{H\beta} > 5$ may bias us toward massive galaxies with abnormally high gas fractions. However, at fixed equivalent width (EW) the distribution of S/N values is broad. Galaxies with $H\beta$ EW $< 5 \text{ \AA}$ have a median $(S/N)_{H\beta}$ of 11, and more than 10% of them have $(S/N)_{H\beta} > 20$. Thus our cuts on S/N are not imposing stringent cuts on EW or gas fraction. We have also done the straightforward experiment of altering the S/N cuts on all our lines and re-fitting the mass–metallicity relation: its detailed shape is insensitive to factor of 2 changes in our S/N cuts.

The most remarkable feature of the stellar mass–metallicity relation is the tightness of the correlation – the 1σ spread of the data about the median ranges from 0.20 dex at low mass to 0.07 dex at high mass. For comparison, the median errors in mass and metallicity are 0.09 dex and 0.03 dex respectively. Adding these appropriately, we find that roughly half of the spread in the mass–metallicity relation can be attributed to observational error. With our large statistical sample we can test whether there is a physical origin for the scatter, even if we have underestimated our measurement errors. In Figure 7 we show the residuals from our fit to the mass–metallicity relation as a function of various galaxy physical properties.

There is a clear tendency for the metallicity residuals to correlate with local surface mass density measured within the fiber aperture. Analogous trends were identified by Bell & de Jong (2000) using resolved photometry of a sample of nearby disk galaxies. They demonstrated that mean stellar metallicity and stellar age correlate with local K-band surface density and concluded that surface density plays a strong role in shaping both the local and global star formation history of a galaxy. Kauffmann et al. (2003b) showed that the star formation histories of low mass galaxies are more fundamentally related to surface mass density than to stellar mass. These findings suggest that at fixed mass, galaxies with higher surface densities have transformed more of the available gas into stars, thereby raising the gas-phase metallicity. This interpretation is borne out by the fact that the residuals also correlate somewhat with galaxy color. But curiously, the same trend is not seen with $H\alpha$ EW or galaxy morphology as measured by the concentration index. This leaves us with a somewhat contradictory picture since these quantities are expected to relate

to a galaxy’s gas content and general evolutionary state.

The other pronounced correlation seen in Figure 7 is between metallicity and inclination, as measured by the ratio of the galaxy minor and major axes. At fixed mass, fully edge-on galaxies ($b/a \sim 0.2$) are more metal poor than face-on galaxies by 0.19 dex. This trend is easily explained because more of the disk is seen in projection in our fiber aperture at higher inclinations. The integrated metallicity decreases as larger galaxy radii are probed because the outer regions of disks tend to be more metal-poor, as well as more gas rich and less extinguished.

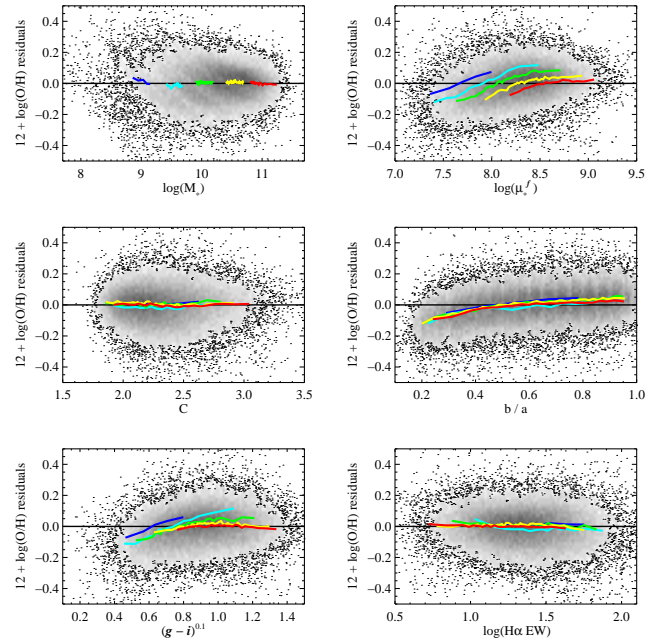


FIG. 7.— Correlation of the residuals of the mass–metallicity relation with various galaxy physical parameters: M_* , the stellar mass in units of M_\odot ; μ_*^f , the local surface mass density measured within the fiber aperture in units of $M_\odot \text{ kpc}^{-2}$; C , the concentration parameter, a proxy for galaxy morphology; b/a , the ratio of the galaxy minor and major axes, a proxy for inclination; $(g-i)$ color k -corrected to $z=0.1$; and $H\alpha$ equivalent width in \AA . The colored lines show the median relation in 5 different mass bins.

6. THE ORIGIN OF THE MASS–METALLICITY RELATION

The existence of a tight (± 0.1 dex) correlation between stellar mass and metallicity reflects the fundamental role that galaxy mass plays in galactic chemical evolution. However, it is not a priori clear whether this sequence is one of enrichment or of depletion. Simply put, if more massive galaxies form fractionally more stars in a Hubble time than their low-mass counterparts, then the observed mass–metallicity relation represents a sequence in astration. However, if galaxies form similar fractions of stars, then the relation could imply that metals are selectively lost from galaxies with small potential wells via galactic winds.

Both of these ideas have a long history in the astronomical literature. It is well known that there are systematic trends in the star formation history of galaxies along the Hubble sequence (e.g. Roberts & Haynes 1994). Recent observations have confirmed that gas mass fractions decrease with increasing stellar mass (McGaugh & de Blok 1997; Bell & de Jong 2000; Boselli, Gavazzi, Donas, & Scodreggio 2001), a trend that seems to suggest that low mass galaxies are un-enriched

rather than depleted. However, observations of starbursts have revealed the nearly ubiquitous presence of galactic winds (Heckman 2002), while studies of X-ray bright clusters have demonstrated the presence of copious metals in the intra-cluster medium (Gibson, Loewenstein, & Mushotzky 1997), and absorption line studies have revealed metals in the intergalactic medium (Ellison, Songaila, Schaye, & Pettini 2000). Given the existence of these contradictory pieces of information, anecdotal arguments are of little use: a direct test of the origin of the mass–metallicity relation is required.

The effects of astration and mass loss on the relationship between mass and metallicity can be disentangled in principle if information on the relative mass of the gas and stars is available. Simple closed box chemical evolution models predict that metallicity (Z) is a simple function of the stellar yield, y , and of the gas mass fraction, μ_{gas} :

$$Z = y \ln(\mu_{\text{gas}}^{-1}) \quad (4)$$

Following Garnett (2002), we assume that the stellar yield is constant. Metallicity is then straightforwardly related to the gas mass fraction if the tenets of the simple model apply – namely that there are no gas inflows or outflows. We can invert Equation 1 to define the ‘effective yield’, which can be computed from the observed metallicity and gas mass fraction. When the simple model applies, the effective yield will equal the true yield, independent of galaxy mass. This straightforward observational test was performed by Garnett (2002) using a sample of 44 nearby spiral and irregular galaxies. Garnett found the effective yield to be constant for galaxies with rotational velocities in excess of $\sim 150 \text{ km s}^{-1}$ and to decline by a factor of ~ 15 below this threshold.

While our SDSS dataset is much larger than the nearby sample of Garnett, we do not have direct information about the H I and H₂ gas content of our galaxies. However, we do have indirect information, by virtue of the fact that all of our sample galaxies are actively forming stars. To estimate the gas mass, we invoke another well known empirical correlation – the Schmidt star formation law (Schmidt 1959; Kennicutt 1998) which relates the star formation surface density to the gas surface density.

For each of our galaxies we calculate the star formation rate (SFR) in the fiber aperture from the attenuation-corrected H α luminosity following Brinchmann et al. (2004). We multiply our SFRs by a factor of 1.5 to convert from a Kroupa (2001) IMF to the Salpeter IMF used by Kennicutt (1998). Our SDSS galaxies have star formation surface densities which are within a factor of 10 of $\Sigma_{\text{SFR}} = 0.3 \text{ M}_{\odot} \text{ yr}^{-1} \text{ kpc}^{-2}$, exactly the range found by Kennicutt (1998) for the central regions of normal disk galaxies. We convert star formation surface density to surface gas mass density, Σ_{gas} , by inverting the composite Schmidt law of Kennicutt (1998),

$$\Sigma_{\text{SFR}} = 1.6 \times 10^{-4} \left(\frac{\Sigma_{\text{gas}}}{1 \text{ M}_{\odot} \text{ pc}^{-2}} \right)^{1.4} \text{ M}_{\odot} \text{ yr}^{-1} \text{ kpc}^{-2}. \quad (5)$$

(Note that the numerical coefficient has been adjusted to include helium in Σ_{gas} .) Combining our spectroscopically derived M/L ratio with a measurement of the z -band surface brightness in the fiber aperture, we compute Σ_{star} , the stellar surface mass density. The gas mass fraction is then $\mu_{\text{gas}} = \Sigma_{\text{gas}} / (\Sigma_{\text{gas}} + \Sigma_{\text{star}})$.

In Figure 8 we plot the effective yield of our SDSS star forming galaxies as a function of total baryonic (stellar + gas) mass. Baryonic mass is believed to correlate with dark

mass, as evidenced by the existence of a baryonic ‘Tully-Fisher’ relation (McGaugh, Schombert, Bothun, & de Blok 2000; Bell & de Jong 2001). We are interested in the dark mass because departures from the ‘closed box’ model might be expected to correlate with the depth of the galaxy potential well. Because very few of our SDSS galaxies have masses below $10^{8.5} \text{ M}_{\odot}$, we augment our data set with measurements from Lee, McCall, & Richer (2003), Garnett (2002), and Pilyugin & Ferrini (2000), *all of which use direct gas mass measurements*. We note that the correspondence between the SDSS data and the samples from the literature is very good in spite of the fact that the gas masses have been determined in very different ways.

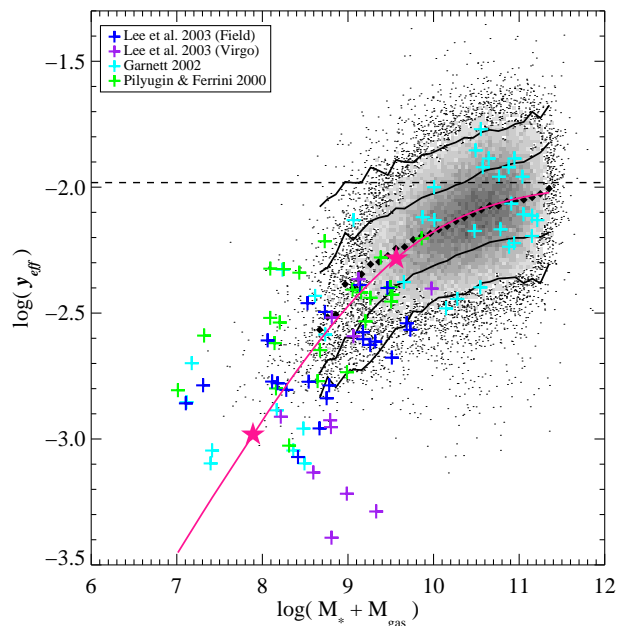


FIG. 8.— Effective yield as a function of total baryonic mass (stellar + gas mass) for 53,400 star-forming galaxies in the SDSS. The large black points represent the median of the SDSS data in bins of 0.1 dex in mass which include at least 100 data points. The solid lines are the contours which enclose 68% and 95% of the data. The colored crosses are data from Lee, McCall, & Richer 2003, Garnett 2002, and Pilyugin & Ferrini 2000. Both the metallicities and the gas masses used to derive the effective yield have been computed differently in the SDSS data and the samples from the literature. The agreement nevertheless appears quite good. The pink line is the best fit to the combined dataset assuming the intrinsic functional from given by Equation 6. The dashed line indicates y_0 , the true yield if no metals are lost, derived from the fit to the data. The pink stars denote galaxies which have lost 50% and 90% of their metals. Data for the contours are given in Table 4.

With the addition of the data from the literature it is clear that galaxies do not evolve as ‘closed boxes’. Figure 8 shows that baryonic mass and effective yield are highly correlated, with the effective yield decreasing by a factor of ~ 10 from the most massive galaxies to dwarfs. The correlation is steep at low masses but begins to flatten around $10^{9.5} \text{ M}_{\odot}$. In §8 we argue that the relationship between effective yield and baryonic mass is the consequence of metal loss via galactic winds. We fit the combined dataset with a simple function predicated on this basis. We assume that the fraction of newly synthesized metals retained by a galaxy is proportional to the depth of the galaxy’s potential well for low mass galaxies, but asymptotes to unity for the most massive systems. The depth of the galaxy potential well scales approximately as V_c^2 , where V_c is

the galaxy circular velocity. We model the retained fraction as $f_{ret} = V_c^2 / (V_c^2 + V_0^2)$ where V_0 is a constant. ($f_{ret}(V_c < V_0) < 0.5$, $f_{ret}(V_c \gg V_0) \sim 1$.) We adopt $M_{baryon} \propto V_c^{3.5}$ from the baryonic Tully-Fisher relation of Bell & de Jong (2001). The effective yield and the baryonic mass may then be related follows:

$$y_{eff} = \frac{y_0}{(1 + (M_0/M_{baryon})^{0.57})} \quad (6)$$

The free parameters of the fit are y_0 , the true yield (if no metals are lost), and M_0 , the mass at which a galaxy loses 1/2 of its metals. We perform the fit to a combination of the SDSS data (the median value of y_{eff} in bins of 0.1 in M_{baryon}) and the data drawn from the literature, applying weights such that both datasets contribute equally to the fit. We find $y_0 = 0.0104$ and $M_0 = 3.67 \times 10^9 M_\odot$. This characteristic mass corresponds to a rotation speed of $V_c = 85 \text{ km s}^{-1}$ and, following Heckman, Lehnert, Strickland, & Armus (2000), an escape velocity of $V_{esc} \sim 3V_c = 260 \text{ km s}^{-1}$. Thus, the escape velocity of a galaxy that has lost half of its metals is just below the observed terminal velocity of starburst winds, which are 300 - 900 km s^{-1} (Heckman, Lehnert, Strickland, & Armus 2000).

The scatter in the correlation between effective yield and baryonic mass is ± 0.15 dex, 50% larger than that measured for the mass-metallicity relation. However, much of the scatter in the SDSS data can probably be ascribed to our relatively uncertain measurement of the gas mass. We note that this does not effect the total mass greatly, as the median gas mass fraction of our sample is $\sim 20\%$. It is interesting to note that galaxies with direct gas mass measurements show comparable scatter, however the stellar mass determinations for these galaxies are correspondingly more uncertain. It is therefore premature to consider a physical origin for the scatter, although it is quite likely that there may be one, for instance differences in galaxy environment (Skillman, Kennicutt, Shields, & Zaritsky 1996; Lee, McCall, & Richer 2003).

7. SOURCES OF SYSTEMATIC ERROR

Galaxies are known to have radial gradients in their physical properties (e.g. Bell & de Jong 2000). Aperture effects are therefore a potentially serious concern because strong selection effects are inherent in magnitude-limited surveys such as the SDSS. For our sample, the median projected fiber size is ~ 4.6 kpc in diameter, with the range extending from 1 to 12 kpc. Thus while we are not measuring ‘nuclear’ spectra, we are clearly not measuring integrated spectra either. The median fraction of galaxy light in the fiber aperture is 24%. Fortunately, because larger galaxies are brighter, they get selected out to larger distances and observed with larger projected apertures. The net effect is that the fraction of galaxy light seen by the fibers is not a strong function of absolute magnitude, as shown in the top panel of Figure 9. Hence, while aperture effects are important in the absolute sense, they are unlikely to have a significant effect on trends with galaxy mass.

Because of the magnitude-limited nature of the SDSS, it is not possible to examine the impact of aperture size simply by comparing galaxies in narrow bins of absolute magnitude at different redshifts. Instead we divide our sample into four broad bins of absolute magnitude and examine trends in galaxy properties as a function of relative redshift, z/z_{max} , where z_{max} is the redshift at which a given galaxy reaches the spectroscopic survey limits. The effect of aperture bias on galaxy M/L ratios was examined as a function

of z/z_{max} by Kauffmann et al. (2003a, see Fig. 18) and found to be ~ 0.1 dex. The strongest trends were observed for L^* galaxies which presumably have both a well developed bulge and a disk. The effect of aperture bias on our measured metallicity is shown in Figure 9. We find a change of at most -0.11 dex in metallicity as galaxies move from one edge of the survey to the other, indicating that our metallicity determinations are only moderately affected by changes in the projected aperture size. This gradient is in good accord with our expectations based on the known radial metallicity gradients in spiral galaxies (Vila-Costas & Edmunds 1992; Zaritsky, Kennicutt, & Huchra 1994; Martin & Roy 1994; van Zee et al. 1998).

While it is desirable to correct our metallicity measurements to reflect true global abundances, it is not possible to derive this correction directly from the SDSS data because even at the limits of the survey the fiber aperture only contains about 50% of a galaxy’s light. Work is under way to obtain the observations necessary for such an analysis. In the meantime, we simply note that because the fibers generally cover the inner few kpc of galaxies, the abundances we derive are likely to be higher than true integrated abundances. Recent evidence also suggests that oxygen abundances derived from ‘strong lines’ methods like ours may overestimate the true abundance by as much as factor of two (Kennicutt, Bresolin, & Garnett 2003).

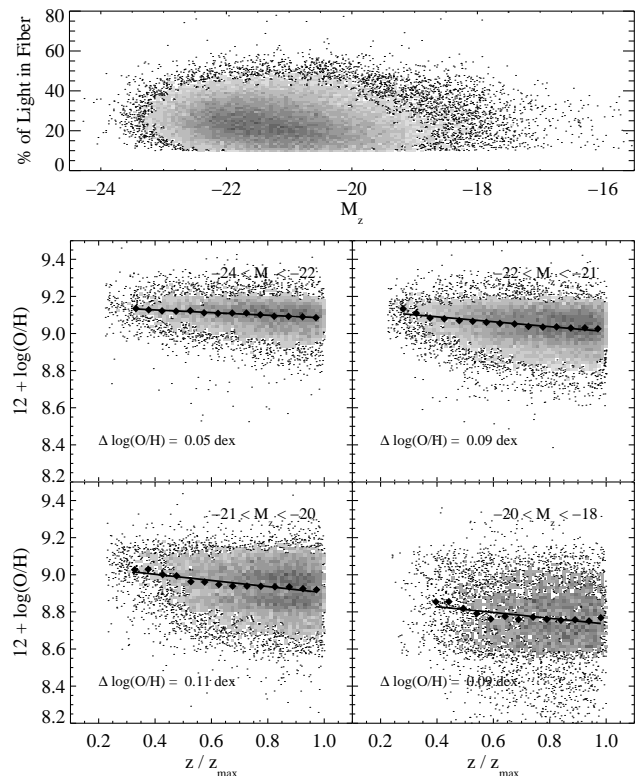


FIG. 9.— A test for aperture bias. In the top panel the fraction of r -band galaxy light observed by the fiber is plotted as a function of absolute magnitude. In the lower panel, metallicity is plotted in 4 broad bins of absolute magnitude as a function of relative redshift, z/z_{max} , where z_{max} is the redshift at which a given galaxy reaches the survey limits. The large black points represent the median; the solid line is a linear fit to the points. The maximum change in metallicity with z/z_{max} (based on the fitted line) is given in the lower left of each panel.

Another potential source of error is our indirect method of

deriving the gas mass from the $H\alpha$ luminosity via the global Schmidt law of Kennicutt (1998). While the impressive correlation between the surface mass density of gas and the surface density of star formation holds over 5 orders of magnitude, there is a fair amount of scatter evident in the narrow regime applicable to the present study (Kennicutt 1998, see Fig. 6). Systematic errors are a bigger concern. Wong & Blitz (2002) found that application of a radially-dependent attenuation correction to $H\alpha$ produced a steeper Schmidt law, with a power law index of 1.7 (as compared to Kennicutt’s 1.4). However, adopting the steeper Schmidt law in our analysis produces a relatively small change in the correlation between baryonic mass and effective yield: $\log y_0$ decreases by 0.04 dex, and $\log M_0$ decreases by 0.15 dex.

Beyond the issue of the accuracy of our μ_{gas} measurement, there is the larger question of whether the central gas mass fraction is the *relevant* gas mass fraction. If $\Sigma_{gas}/\Sigma_{star}$ varies strongly with radius, than our measurements are unlikely to be representative of the galaxy as a whole. These concerns are allayed to some degree by the generally strong correspondence seen between $H\alpha$ and broad-band optical disk scale lengths (Hodge & Kennicutt 1983; Kennicutt 1989). A more fundamental question, however, is how the products of star formation are distributed in galaxies – in other words, how well mixed is the interstellar medium? The mere existence of radial metallicity gradients in spirals suggests that mixing timescales are generally long. In this case, local abundances reflect local astration levels, and hence the relevant gas mass fraction is the local one. A final issue is the existence of cold gas external to the stellar disk in some galaxies. It is unclear whether this gas is relevant to our calculation, since it does not strongly participate in the star formation. However, if the outlying gas viscously mixes with gas in the inner disk it would affect the observed metallicity, and should be included in the gas budget. In any case, since we have no information on the extended gas in our galaxies, we do not consider it at present, except to note that its inclusion would raise our measured value of the effective yield. For galaxies with baryonic masses of $10^7 M_\odot$ the gas mass would need to increase by a factor of ~ 11 to erase the signatures of metal loss.

While the sources of systematic error cannot be ignored, we believe the magnitude of these errors to be small, on the order of a few tenths of a dex. In view of the moderately large dynamic range of our results – a factor of ~ 10 decrease in both metallicity and effective yield – our general result, the preferential loss of metals from galaxies with small potential wells, appears very robust. Future observations which spatially resolve the distribution of gas and metals in galaxies will prove key to understanding many of the relevant systematic effects.

8. SUMMARY & DISCUSSION

We have coupled advanced techniques for deriving stellar masses and gas-phase metallicities from optical spectroscopy and photometry with the statistical power provided by the SDSS. For a sample of 53,400 star-forming galaxies at $z \sim 0.1$, we find a tight correlation (± 0.1 dex) between stellar mass and the gas-phase oxygen abundance, which extends over 3 orders of magnitude in stellar mass and a factor of 10 in oxygen abundance. We use indirect estimates of the gas mass fraction based on our measured $H\alpha$ luminosity to estimate the effective yield. Simple closed box chemical evolution models predict that the effective yield is constant. Combining our SDSS data with data from the literature, we find evidence that the effective yield decreases by a factor of ~ 10 from the most

massive galaxies to dwarfs.

The most straightforward interpretation of the correlation between baryonic mass and effective yield is the selective loss of metals from galaxies with shallow potential wells via galactic winds, an idea first introduced by Larson (1974). Evidence for galactic outflows has steadily accumulated from observations at optical (Lehnert & Heckman 1996; Heckman, Lehnert, Strickland, & Armus 2000), X-ray, (Dahlem, Weaver, & Heckman 1998; Martin, Kobulnicky, & Heckman 2002), and ultraviolet wavelengths (Heckman & Leitherer 1997; Pettini, et al. 2000). However, comparatively little is known about the eventual *fate* of the wind material — whether it escapes from the galaxy potential, or cools and eventually rains back down on the disk. A number of arguments have been made to this effect. Heckman, Lehnert, Strickland, & Armus (2000) found the terminal velocity of starburst-driven winds to be $300\text{--}900 \text{ km s}^{-1}$, independent of the host galaxy properties, and invoked simple models of the gravitational potential to suggest that galactic outflows escape from the potential wells of dwarf galaxies, but not from more massive hosts. However these simple scaling arguments neglect the multi-phase nature of galactic winds, and the complicated interaction of the wind with the interstellar medium of the disk and the halo. Drawing on the numerical simulations of Mac Low & Ferrara (1999) which attempt to include this complicated gas physics, Ferrara & Tolstoy (2000) conclude that galaxies with gas masses greater than $\sim 10^9 M_\odot$ do not experience outflows. In contrast, our results imply that galaxies with masses as high as $10^{10} M_\odot$ still eject some fraction of their metals into the intergalactic medium. This result is in line with the recent observational and theoretical work of Strickland et al. (2003). These authors suggest that blowout is possible from galaxies with masses as high as $10^{11} M_\odot$ based on a model where supernovae in disk OB associations work together to power the outflow.

Of course it is quite likely that even in the absence of winds chemical evolution does not proceed in the simple manner we have assumed. It is worth considering if other factors could explain the trends we observe. For example, another means of lowering the effective yield is the inflow of metal-poor gas. While inflow may occur in some galaxies (the Milky Way, for instance) we do not regard it as a viable explanation for the correlation between effective yield and baryonic mass. Metal-poor inflow acts to lower the metallicity and to raise the gas mass fraction, so the net effect on the effective yield is modest. For example, consider a galaxy presently undergoing closed box chemical evolution with a gas fraction of 0.3. If such a galaxy experiences an inflow of metal-free gas with a mass equal to its present gas mass, the metallicity is reduced by 50%, the gas mass fraction is increased by 54%, and the effective yield is decreased by 22% ($\Delta \log y_{eff} = 0.1$ dex). Thus, even dramatic inflow events have only a moderate effect on the effective yield. Garnett (2002) pointed out that the low effective yields of the smallest dwarfs would require them to accrete as much as 80-90% of their gas at late times without experiencing much star formation. We therefore consider it unlikely that metal-poor inflow is solely responsible for the low yields we observe.

Another factor that can lower the effective yield is a breakdown of the instantaneous recycling approximation – the assumption that gas is either immediately enriched and returned to the ISM or locked up forever in low mass stars. While this assumption obviously does not hold in detail, the main prac-

tical concern is at late times when low mass stars return their comparatively un-enriched gas to the interstellar medium. If this were a chemically significant effect then we would expect the effective yield to decrease as a function of mean galaxy age. Kauffmann et al. (2003b, see Fig. 1) demonstrated a tight correlation between stellar mass and the $D_n(4000)$ spectral index, which is a good tracer of the mean stellar age of a population. The correlation is in the sense that more massive galaxies appear to be older. Hence we would predict that y_{eff} should decrease with galaxy mass, just the opposite of what is seen. While gas recycling may indeed influence the detailed shape of the $y_{eff} - M_{baryon}$ relation, it is almost certainly not the main driver of the observed trend.

It is our view that the strong positive correlation between effective yield and baryonic mass is most *naturally* explained by the increasing potential barrier which the metal-laden wind must overcome to achieve ‘blow out’. While the correlation is not particularly tight (± 0.15 dex), its very existence nevertheless implies two very interesting things. First, nearly all low mass galaxies and many high mass galaxies have experienced some sort of blow-out event. Since the energy requirements for blow-out are fairly exacting, it seems likely that these events are associated with starburst activity. This chain of reasoning leads us to suggest that the star formation histories of *most* galaxies may be bursty rather than continuous. (However, see Skillman (2001), van Zee (2001), and Hunter & Gallagher (1985) for some opposing viewpoints.) Unfortunately too little is known about the extended gaseous halos of normal galaxies and the conditions required for blow-out to make a more quantitative statement (see Strickland et al. 2003). The second significant implication is that blow-out events have an important chemical impact even when integrated over a galaxy’s history of star formation. This suggests that blow-out is either a very frequent occurrence or very catastrophic. In the coming years numerical and semi-analytical models should help to address these questions. In the meantime we emphasize our empirical findings: galactic winds are ubiquitous and extremely effective in removing metals from galaxies.

The quest to understand how the chemical properties of galaxies couple to their star formation histories has been given added impetus of late by measurements of the metallicity-luminosity relation of galaxies at intermediate ($0.3 < z < 1.0$) (Kobulnicky et al. 2003; Lilly, Carollo, & Stockton 2003; Maier, Meisenheimer, & Hippelein 2004) and high ($z > 2$) redshifts (Kobulnicky & Koo 2000; Pettini et al. 2001). Our results imply that metallicity is not a straightforward metric of galaxy evolution because metals can escape galactic potential wells. However, the strong correspondence of metal loss with the size of the potential has interesting implications if effective yields can be measured reliably. The combination of the intermediate and high redshift data with the correlations we measure at $z \sim 0.1$ will provide an important benchmark for successful models of feedback and galaxy evolution.

The authors wish to thank John Moustakas, Rob Kennicutt, and Roberto Terlevich for useful discussions, Dave Strickland for helpful ‘feedback’ on the text, and Larry Bradley for his assistance with our IDL code. We gratefully acknowledge the referee, Evan Skillman, for insightful comments that improved the paper. The data processing software developed for this project benefited from IDL routines written by Craig Markwardt and from the IDL Astronomy User’s

Library maintained by Wayne Landsman at Goddard Space Flight Center. C. A. T. thanks the Max Planck Institute for Astrophysics and the Johns Hopkins Center for Astrophysics for their generous financial support. She also acknowledges support from NASA grant NAG 58426 and NSF grant AST-0307386. J. B. and S. C. thank the Alexander von Humboldt Foundation, the Federal Ministry of Education and Research, and the Programme for Investment in the Future (ZIP) of the German Government for their support. J. B. would also like to acknowledge the receipt of an ESA post-doctoral fellowship.

Funding for the creation and distribution of the SDSS Archive has been provided by the Alfred P. Sloan Foundation, the Participating Institutions, the National Aeronautics and Space Administration, the National Science Foundation, the U.S. Department of Energy, the Japanese Monbukagakusho, and the Max Planck Society. The SDSS Web site is <http://www.sdss.org/>. The SDSS is managed by the Astrophysical Research Consortium (ARC) for the Participating Institutions. The Participating Institutions are The University of Chicago, Fermilab, the Institute for Advanced Study, the Japan Participation Group, The Johns Hopkins University, Los Alamos National Laboratory, the Max-Planck-Institute for Astronomy (MPIA), the Max-Planck-Institute for Astrophysics (MPA), New Mexico State University, University of Pittsburgh, Princeton University, the United States Naval Observatory, and the University of Washington.

REFERENCES

- Allende Prieto, C., Lambert, D. L., & Asplund, M. 2001, *ApJ*, 556L
- Alloin, D., Collin-Souffrin, S., Joly, M., & Vigroux, L. 1979, *A&A*, 78, 200
- Abazajian, K. et al. 2004, *AJ*, in press
- Baldwin, J. A., Phillips, M. M., & Terlevich, R. 1981, *PASP*, 93, 5
- Bell, E. F. & de Jong, R. S. 2000, *MNRAS*, 312, 497
- Bell, E. F. & de Jong, R. S. 2001, *ApJ*, 550, 212
- Boselli, A., Gavazzi, G., Donas, J., & Scodreggio, M. 2001, *AJ*, 121, 753
- Brinchmann, J. & Ellis, R. S. 2000, *ApJ*, 536, L77
- Brinchmann, J., Charlot, S., White, S. D. M., Tremonti, C., Kauffmann, G., Heckman, T., Brinkmann, J. 2004, *MNRAS*, accepted
- Bruzual G. & Charlot, S. 1993, *ApJ*, 405, 538
- Bruzual, G. & Charlot, S., *MNRAS*, accepted
- Blanton, M. R., Lin, H., Lupton, R. H., Maley, F. M., Young, N., Zehavi, I., & Loveday, J. 2003, *AJ*, 125, 2276
- Blanton, M. R., Brinkmann, J., Csabai, I., Doi, M., Eisenstein, D., Fukugita, M., Gunn, J. E., Hogg, D. W., & Schlegel, D. J. 2003, *AJ*, 125, 2348
- Brodie, J. P. & Huchra, J. P. 1991, *ApJ*, 379, 157
- Charlot, S. et al. 2004, in preparation
- Charlot, S. & Longhetti, M. 2001, *MNRAS*, 323, 887
- Charlot, S. & Fall, S. M. 2000, *ApJ*, 539, 718
- Contini, T., Treyer, M. A., Sullivan, M., & Ellis, R. S. 2002, *MNRAS*, 330, 75
- Coziol, R., Contini, T., Davoust, E., & Considere, S. 1997, *ApJ*, 481, L67
- Dahlem, M., Weaver, K. A., & Heckman, T. M. 1998, *ApJS*, 118, 401
- Dopita, M. A. & Evans, I. N. 1986, *ApJ*, 307, 431
- Edmunds, M. G. & Pagel, B. E. J. 1984, *MNRAS*, 211, 507
- Ellison, S. L., Songaila, A., Schaye, J., & Pettini, M. 2000, *AJ*, 120, 1175
- Ferland, G. 1996, *Hazy, A Brief Introduction to Cloudy*. Internal Report, University of Kentucky, USA
- Ferrara, A. & Tolstoy, E. 2000, *MNRAS*, 313, 291
- Frye, B., Broadhurst, T., & Benítez, N. 2002, *ApJ*, 568, 558
- Fukugita, M., Ichikawa, T., Gunn, J. E., Doi, M., Shimasaku, K., & Schneider, D. P. 1996, *AJ*, 111, 1748
- Garnett, D. R. 1999, *IAU Symp. 190: New Views of the Magellanic Clouds*, 190, 266
- Garnett, D. R. 2002, *ApJ*, 581, 1019
- Garnett, D. R. & Shields, G. A. 1987, *ApJ*, 317, 82
- Gibson, B. K., Loewenstein, M., & Mushotzky, R. F. 1997, *MNRAS*, 290, 623
- Gunn, J. E. et al. 1998, *AJ*, 116, 3040
- Heckman, T. M. & Leitherer, C. 1997, *AJ*, 114, 69
- Heckman, T. M., Lehnert, M. D., Strickland, D. K., & Armus, L. 2000, *ApJS*, 129, 493
- Heckman, T. M. 2002, *ASP Conf. Ser. 254: Extragalactic Gas at Low Redshift*, 292
- Hodge, P. W. & Kennicutt, R. C. 1983, *ApJ*, 267, 563
- Hogg, D. W., Finkbeiner, D. P., Schlegel, D. J., and Gunn, J. E. 2001, *AJ*, 122, 2129
- Hunter, D. A. & Gallagher, J. S. 1985, *ApJS*, 58, 533
- Isobe, T., Feigelson, E. D., Akritas, M. G., & Babu, G. J. 1990, *ApJ*, 364, 104
- Kauffmann, G. et al. 2003a, *MNRAS*, 341, 33
- Kauffmann, G. et al. 2003b, *MNRAS*, 341, 54
- Kauffmann, G. et al. 2003c, *MNRAS*, 346, 1055
- Kennicutt, R. C., Jr. 1989, *ApJ*, 344, 685
- Kennicutt, R. C., Jr. 1998, *ApJ*, 498, 541
- Kennicutt, R. C., Jr., Bresolin, F. & Garnett, D. R. 2003, *ApJ*, 591, 801
- Kewley, L. J. & Dopita, M. A. 2002, *ApJS*, 142, 35
- Kewley, L. J., Dopita, M. A., Sutherland, R. S., Heisler, C. A., & Trevena, J. 2001, *ApJ*, 556, 121
- Kobulnicky, H. A. & Zaritsky, D. 1999, *ApJ*, 511, 118
- Kobulnicky, H. A., Kennicutt, R. C., & Pizagno, J. L. 1999, *ApJ*, 514, 544
- Kobulnicky, H. A. & Koo, D. C. 2000, *ApJ*, 545, 712
- Kobulnicky, H. et al. 2003, *ApJ*, submitted
- Kroupa, P. 2001, *MNRAS*, 322, 231
- Larson, R. B. 1974, *MNRAS*, 169, 229
- Larson, R. B. & Dinerstein, H. L. 1975, *PASP*, 87, 911
- Le Borgne, J. -F., Bruzual, G., Pelló, R., Lançon, A., Rocca-Volmerange, B., Sanahuja, B., Schaerer, D., Soubiran, C., Vílchez-Cómez, in preparation
- Lee, H., McCall, M. L., & Richer, M. G. 2003, *AJ*, 125, 2975
- Lehnert, M. D. & Heckman, T. M. 1996, *ApJ*, 472, 546
- Lequeux, J., Rayo, J. F., Serrano, A., Peimbert, M., & Torres-Peimbert, S. 1979, *A&A*, 80, 155
- Lilly, S. J., Carollo, C. M., & Stockton, A. N. 2003, *ApJ*, in press
- Mac Low, M. & Ferrara, A. 1999, *ApJ*, 513, 142
- Martin, C. L., Kobulnicky, H. A., & Heckman, T. M. 2002, *ApJ*, 574, 663
- Martin, P. & Roy, J. 1994, *ApJ*, 424, 599
- Martin, C. L. 1997, *ApJ*, 491, 561
- McCall, M. L., Rybski, P. M., & Shields, G. A. 1985, *ApJS*, 57, 1
- McGaugh, S. S. 1991, *ApJ*, 380, 140
- McGaugh, S. S. & de Blok, W. J. G. 1997, *ApJ*, 481, 689
- McGaugh, S. S., Schombert, J. M., Bothun, G. D., & de Blok, W. J. G. 2000, *ApJ*, 533, L99
- Melbourne, J. & Salzer, J. J. 2002, *AJ*, 123, 2302
- Maier, C., Meisenheimer, K., & Hippelein, H. 2004, *A&A*, 418, 475
- Pagel, B. E. J., Edmunds, M. G., Blackwell, D. E., Chun, M. S., & Smith, G. 1979, *MNRAS*, 189, 95
- Pettini, M., Steidel, C. C., Adelberger, K. L., Dickinson, M., & Giavalisco, M. 2000, *ApJ*, 528, 96
- Pettini, M., Shapley, A. E., Steidel, C. C., Cuby, J., Dickinson, M., Moorwood, A. F. M., Adelberger, K. L., & Giavalisco, M. 2001, *ApJ*, 554, 981
- Pier, J.R., Munn, J.A., Hindsley, R.B., Hennessy, G.S., Kent, S.M., Lupton, R.H., and Ivezić, Z. 2003, *AJ*, 125, 1559 (*Astrometry*)
- Pilyugin, L. S. & Ferrini, F. 2000, *A&A*, 354, 874
- Richer, M. G. & McCall, M. L. 1995, *ApJ*, 445, 642
- Roberts, M. S. & Haynes, M. P. 1994, *ARA&A*, 32, 115
- Rupke, D. S., Veilleux, S., & Sanders, D. B. 2002, *ApJ*, 570, 588
- Schlegel, D. J., Finkbeiner, D. P., & Davis, M. 1998, *ApJ*, 500, 525
- Schmidt, M. 1959, *ApJ*, 129, 243
- Shapley, A. E., Steidel, C. C., Adelberger, K. L., Dickinson, M., Giavalisco, M., & Pettini, M. 2001, *ApJ*, 562, 95
- Shimasaku, K. et al. 2001, *AJ*, 122, 1238
- Skillman, E. D. 2001, *Astrophysics and Space Science Supplement*, 277, 383
- Skillman, E. D., Kennicutt, R. C., Shields, G. A., & Zaritsky, D. 1996, *ApJ*, 462, 147
- Skillman, E. D., Kennicutt, R. C., & Hodge, P. W. 1989, *ApJ*, 347, 875
- Smith, J. A. et al. 2002, *AJ*, 123, 2121
- Stoughton, C. et al. 2002, *AJ*, 123, 485
- Strateva, I. et al. 2001, *AJ*, 122, 1861
- Strauss, M. A. et al. 2002, *AJ*, 124, 1810
- Strickland, D. K., Heckman, T. M., Colbert, E. J. M., Hoopes, C. G., & Weaver, K. A., *ApJ*, submitted
- Strickland, D. K., Heckman, T. M., Weaver, K. A., Hoopes, C. G., & Dahlem, M. 2002, *ApJ*, 568, 689
- Strickland, D. K. & Stevens, I. R. 2000, *MNRAS*, 314, 511
- Thilker, D. A., Walterbos, R. A. M., Braun, R., & Hoopes, C. G. 2002, *AJ*, 124, 3118
- Tully, R. B., Pierce, M. J., Huang, J., Saunders, W., Verheijen, M. A. W., & Witchalls, P. L. 1998, *AJ*, 115, 2264
- van Zee, L. 2001, *AJ*, 121, 2003
- van Zee, L., Salzer, J. J., Haynes, M. P., O'Donoghue, A. A., & Balonek, T. J. 1998, *AJ*, 116, 2805
- Veilleux, S. & Osterbrock, D. E. 1987, *ApJS*, 63, 295
- Vila-Costas, M. B. & Edmunds, M. G. 1992, *MNRAS*, 259, 121
- White, S. D. M. & Rees, M. J. 1978, *MNRAS*, 183, 341
- Worthey, G. 1994, *ApJS*, 94, 687
- Wong, T. & Blitz, L. 2002, *ApJ*, 569, 157
- York, D. G. et al. 2000, *AJ*, 120, 1579
- Zaritsky, D., Kennicutt, R. C., & Huchra, J. P. 1994, *ApJ*, 420, 87
- Zurita, A., Rozas, M., & Beckman, J. E. 2000, *A&A*, 363, 9

TABLE 1
THE g -BAND LUMINOSITY-METALLICITY
RELATION

M_g	$12 + \log(\text{O}/\text{H})$				
	$P_{2.5}$	P_{16}	P_{50}	P_{84}	$P_{97.5}$
-22.37	8.86	8.99	9.08	9.15	9.26
-21.99	8.88	9.00	9.09	9.15	9.24
-21.61	8.87	8.99	9.09	9.15	9.24
-21.23	8.84	8.97	9.07	9.14	9.23
-20.84	8.77	8.92	9.04	9.13	9.21
-20.45	8.71	8.87	9.01	9.11	9.19
-20.05	8.66	8.82	8.97	9.09	9.17
-19.67	8.60	8.76	8.93	9.07	9.17
-19.26	8.55	8.71	8.89	9.05	9.16
-18.87	8.39	8.64	8.83	9.02	9.14
-18.46	8.32	8.61	8.81	9.00	9.14
-18.07	8.21	8.52	8.70	8.96	9.11
-17.68	8.20	8.41	8.66	8.89	9.12
-17.28	8.18	8.34	8.62	8.87	9.07
-16.87	8.08	8.23	8.49	8.81	9.15

NOTE. — The columns labeled P represent the 2.5, 16, 50, 84, and 97.5 percentile of the distribution of metallicity in bins of 0.4 dex in luminosity. P_{50} is the median. The g -band luminosity is in AB magnitudes and has been corrected for inclination-dependent extinction but not internal extinction.

TABLE 2
THE z -BAND LUMINOSITY-METALLICITY
RELATION

M_z^{cor}	$12 + \log(\text{O}/\text{H})$				
	$P_{2.5}$	P_{16}	P_{50}	P_{84}	$P_{97.5}$
-23.67	9.00	9.06	9.12	9.18	9.29
-23.30	8.95	9.05	9.11	9.18	9.27
-22.91	8.94	9.03	9.11	9.17	9.25
-22.53	8.92	9.01	9.09	9.15	9.24
-22.13	8.87	8.98	9.07	9.14	9.22
-21.74	8.83	8.94	9.04	9.12	9.19
-21.35	8.75	8.88	9.00	9.09	9.17
-20.94	8.70	8.83	8.96	9.06	9.15
-20.56	8.64	8.77	8.90	9.02	9.12
-20.16	8.58	8.70	8.85	8.98	9.10
-19.76	8.47	8.64	8.79	8.94	9.08
-19.36	8.37	8.61	8.73	8.89	9.06
-18.96	8.23	8.52	8.67	8.83	9.04
-18.56	8.15	8.40	8.62	8.78	9.02
-18.18	8.15	8.31	8.57	8.72	8.94
-17.79	8.16	8.24	8.45	8.66	8.87
-17.39	8.04	8.15	8.36	8.59	8.94

NOTE. — The columns labeled P represent the 2.5, 16, 50, 84, and 97.5 percentile of the distribution of metallicity in bins of 0.4 dex in luminosity. P_{50} is the median. The z -band luminosity is in AB magnitudes and has been corrected for internal extinction.

TABLE 3
THE MASS–METALLICITY RELATION

$\log(M_*/M_\odot)$	$12 + \log(\text{O}/\text{H})$				
	$P_{2.5}$	P_{16}	P_{50}	P_{84}	$P_{97.5}$
8.57	8.18	8.25	8.44	8.64	8.77
8.67	8.11	8.28	8.48	8.65	8.84
8.76	8.13	8.32	8.57	8.70	8.88
8.86	8.14	8.37	8.61	8.73	8.89
8.96	8.21	8.46	8.63	8.75	8.95
9.06	8.26	8.56	8.66	8.82	8.97
9.16	8.37	8.59	8.68	8.82	8.95
9.26	8.39	8.60	8.71	8.86	9.04
9.36	8.46	8.63	8.74	8.88	9.03
9.46	8.53	8.66	8.78	8.92	9.07
9.57	8.59	8.69	8.82	8.94	9.08
9.66	8.60	8.72	8.84	8.96	9.09
9.76	8.63	8.76	8.87	8.99	9.10
9.86	8.67	8.80	8.90	9.01	9.12
9.96	8.71	8.83	8.94	9.05	9.14
10.06	8.74	8.85	8.97	9.06	9.15
10.16	8.77	8.88	8.99	9.09	9.16
10.26	8.80	8.92	9.01	9.10	9.17
10.36	8.82	8.94	9.03	9.11	9.18
10.46	8.85	8.96	9.05	9.12	9.21
10.56	8.87	8.98	9.07	9.14	9.21
10.66	8.89	9.00	9.08	9.15	9.23
10.76	8.91	9.01	9.09	9.15	9.24
10.86	8.93	9.02	9.10	9.16	9.25
10.95	8.93	9.03	9.11	9.17	9.26
11.05	8.92	9.03	9.11	9.17	9.27
11.15	8.94	9.04	9.12	9.18	9.29
11.25	8.93	9.03	9.12	9.18	9.29

NOTE. — The columns labeled P represent the 2.5, 16, 50, 84, and 97.5 percentile of the distribution of metallicity in bins of 0.1 dex in stellar mass. P_{50} is the median.

TABLE 4
THE BARYONIC MASS–EFFECTIVE YIELD RELATION

$\log (M_{\text{baryon}}/M_{\odot})$	$\log y_{\text{eff}}$				
	$P_{2.5}$	P_{16}	P_{50}	P_{84}	$P_{97.5}$
8.67	-2.84	-2.74	-2.57	-2.34	-2.08
8.76	-2.75	-2.69	-2.52	-2.32	-2.05
8.86	-2.80	-2.68	-2.51	-2.27	-2.03
8.97	-2.74	-2.60	-2.39	-2.18	-1.98
9.06	-2.72	-2.60	-2.40	-2.21	-1.98
9.16	-2.73	-2.53	-2.35	-2.17	-1.98
9.26	-2.69	-2.49	-2.31	-2.13	-1.92
9.36	-2.65	-2.46	-2.30	-2.12	-1.93
9.47	-2.61	-2.43	-2.27	-2.11	-1.95
9.56	-2.56	-2.39	-2.24	-2.08	-1.89
9.66	-2.55	-2.38	-2.24	-2.09	-1.90
9.76	-2.49	-2.35	-2.21	-2.06	-1.90
9.86	-2.50	-2.33	-2.19	-2.04	-1.87
9.96	-2.46	-2.32	-2.18	-2.03	-1.87
10.06	-2.44	-2.30	-2.17	-2.02	-1.85
10.16	-2.44	-2.29	-2.15	-2.01	-1.83
10.26	-2.43	-2.27	-2.13	-1.99	-1.82
10.36	-2.43	-2.26	-2.12	-1.98	-1.80
10.46	-2.41	-2.25	-2.11	-1.96	-1.80
10.56	-2.38	-2.23	-2.09	-1.94	-1.78
10.66	-2.38	-2.22	-2.07	-1.93	-1.77
10.76	-2.36	-2.21	-2.07	-1.92	-1.78
10.86	-2.36	-2.21	-2.06	-1.91	-1.77
10.95	-2.36	-2.20	-2.05	-1.90	-1.75
11.05	-2.38	-2.20	-2.05	-1.90	-1.74
11.15	-2.36	-2.19	-2.04	-1.88	-1.70
11.25	-2.38	-2.20	-2.03	-1.86	-1.73
11.35	-2.30	-2.18	-2.01	-1.82	-1.68

NOTE. — The columns labeled P represent the 2.5, 16, 50, 84, and 97.5 percentile of the distribution of the effective yield in bins of 0.1 dex in baryonic mass. P_{50} is the median.